Int. J. Electrochem. Sci., 16 **(2021)** Article ID: 210615, doi: 10.20964/2021.06.07

International Journal of
ELECTROCHEMICAL
SCIENCE
www.electrochemsci.org

Effective removal of total organic carbon from soil polluted with agricultural solid waste leachate using electrocoagulation

Xu Han[1,2], *Guangchun Liu*[1,*], *Kun Liu*[2], *Ting Li*[2]

[1] Liaoning Provincial Key Laboratory of Urban Pest Management and Ecological Safety, ShenYang University, ShenYang 110044, China
[2] Green Island Institute of Environmental Resources, ShenYang City University, Shenyang 110112 , China
[*]E-mail: liuguangchun666@sina.com

Received: 2 February 2021 / *Accepted:* 22 March 2021 / *Published:* 30 April 2021

This study focused on treatment of total organic carbon (TOC) and chemical oxygen demand (COD) from soil pollution of agricultural solid waste leachate using electrocoagulation by Al and Fe nanocomposite (Al@Fe) electrodes. Al@Fe was synthesized through an electrodeposition method. Study of morphology and crystalline structure of the sample by SEM and XRD analyses showed that the electrodeposited samples consisted of spherical nanoparticles of Al in fcc crystal structure and Fe in polycrystalline α-iron metallic which homogeneously distributed in the composite matrix. Moreover, the effects of initial pH, current density and Fe concentration in nanocomposite content on electrocoagulation treatment were examined. Results showed COD and TOC removal efficiencies were obtained 95% and 96%, respectively after 60 minutes electrocoagulation treatment in 2 gl^{-1} NaCl as a supporting electrolyte under optimal condition (pH 6) and applied current density of 1mA/cm^2 at room temperature using Al@Fe electrode with equal concentration of Al and Fe. Results indicated that synergetic effect of Al and Fe nanoparticles in nanocomposites electrodes provided the higher effective surface and fast electron transfer rate for electrochemical treatment.

Keywords: Electrocoagulation; Total organic carbon; Chemical oxygen demand; Agricultural solid waste leachate; Nanocomposite

1. INTRODUCTION

Leachate as a high toxic and hazardous pollutant of soil and groundwater is formed in municipal solid waste and landfills [1]. Increasing population, consumerism, industrialization and destruction of natural resources leads to increase in waste production in the world [2]. Today, it is essential to management and control of landfills, the destruction of toxic waste and the treatment of leachate are important. Therefore, many studies have been conducted on the properties of leachates and their treatment [3-7].

Leachates treatments techniques conclude filtration, transfer and recycling of leachate, flotation, ammonium stripping, coagulation–flocculation, ion exchange, adsorption, ozonation, chemical oxidation, electrochemical oxidation, chemical precipitation [8]. Among them, electrocoagulation as electrochemical methods can be a beneficial process for substitution of the conventional leachate treatment process due to economical, energy efficiency and versatility [9]. Material and morphology of electrodes in electrochemical treatment and sensing systems are important factors that can miniaturize the systems and decrease the time and consuming energy [10-12]. Al and Fe electrodes are used extensively in the electrocoagulation process due to cheapness, frequent availability and effectiveness. However, very few studies have been performed on various nanostructured electrodes to promote the treatment process such as aluminum nanoparticles [13], carbon nanotube polytetrafluoroethylene [14], and graphene oxide [15].

Therefore, this study was focused on synthesis and application of nanostructure electrodes for soil pollution of agricultural solid waste leachate using electrocoagulation. Al and Fe nanocomposites were synthesized using electrodeposition technique and studied for treatment of total organic carbon and chemical oxygen demand.

2. EXPERIMENT

Fe@Al nanocomposites were electrodeposited from the ionic liquid 1-butyl-1-methylpyrrolidinium trifluoromethanesulfonate ([$Py_{1,4}$] TfO, 95%, Sigma-Aldrich) [16]. Low-carbon steel (1 cm thickness, Anhui Fitech Materials Co., Ltd., China) and glassy carbon electrode (GCE) were used as a substrate for electrocoagulation and cyclic voltammetry (CV) studies, respectively. Prior to the electrodeposition, the substrate was polished with 600 grit sandpaper (LinyiRunge Building Materials Co., Ltd., China), then immersed in methanol (≥99%, Xilong Scientific Co., Ltd., China) for 10 min. The ionic liquid was further dried for two days at 100°C under vacuum and stored in closed bottles in an argon filled glove box with water and oxygen contents below 2 ppm (OMNI-LAB from Vacuum Atmospheres). The mixture of 1M Aluminum chloride ($AlCl_3$, >99%, Hebei Chisure Biotechnology Co., Ltd., China) and 1M Iron(II) chloride ($FeCl_2$, 90%, AnkangLanzhiguang Environmental Protection Technology Co., Ltd., China) solutions were prepared in 0.1M [$Py_{1,4}$]TfO at 90°C with volume ratio of 1:0, 4:1, 3:1, 1:1, 1:3 and 0:1 which denoted to 0, 20, 25, 50, 75 and 100% of Fe content in Al@Feas Al nanoparticles (Al NPs), Al@Fe (4:1), Al@Fe (3:1), Al@Fe, Al@Fe (1:3) and Fe nanoparticles (Fe NPs) electrodes, respectively. The electrodeposition cell contained the substrate as working electrode. For Al electrodeposition, Al wires were used as reference and counter electrodes. For electrodeposition of Fe and Fe@Al nanocomposites, Pt wires were used as quasi-reference and counter electrodes. The electrodeposition was conducted on galvanostatic conditions using a PARSTAT 2263 potentiostat/galvanostat with a 1 mA/cm^2 current density for 60 minutes at 100°C. The CVs were recorded in a conventional three electrode cell which contained the Fe@Al modified GCE (Fe@Al/GCE) as working electrode, Pt wire as counter and Ag/AgCl as the reference electrode. The electrolyte for CVs measurements was 1mM $K_3[Fe(CN)_6]$ (≥99.0%, Sigma-Aldrich) containing 0.1M KCl (≥99.0%,Sigma-Aldrich). Scanning electron microscopy (SEM; Sigma 500 VP,

Carl Zeiss AG, Germany) and X-ray diffractometer (XRD, X'pert3, PANalytical, The Netherlands) were used to study the morphology and crystalline structure of the samples, respectively.

The leachate was collected from the landfill of agricultural solid waste of Beijing. The average age range of waste in this landfill was over 30 years. Studies have been demonstrated that when the waste passes the maturation step, macromolecules show a great degree of the organic carbon [4, 17, 18].The landfill leachate was treated in using an anaerobic hybrid laboratory-scale digester and nitrogen,and ultrafiltration in a membrane bioreactor, and reverse osmosis process for remove biodegradable organics and filtratration of bio-effluent according to anaerobic treatment of municipal landfill leachate using an anaerobic hybrid digester as following steps [3]: two ultrafiltration module were used to chemical cleaning. The first module was the submerged ultrafiltration membrane module which contained Polyvinylidene fluoride (PVDF, ZeeWeed 500D) hollow fiber membrane with 0.05μm average pore size, 2.0 mm outer diameter, 0.8 mm inner diameter and 1.0 m² total surface area. The aeration system was installed at the bottom, which conducted on a pressure of 0.65 bar, 13L/m^2h permeate flux and a permeate recovery of 90 %. The two-stage anaerobic membrane bioreactors were employed at room temperature which includes two anaerobic reactors. The acidogenic reactor as first reactor was operated in upward flow with a volume of 4.0L and a hydraulic retention time of 10 hours. Methanogenic reactor as the second reactor was operated with a volume of 21L and hydraulic retention time of 48 hours, receiving the acidogenic reactor effluent by gravity. The second ultrafiltration module was conducted on the reactor and submerged ultrafiltration module which contained the PVDF hollow-fiber membrane with 0.05μm pore size and 0.07 m² active membrane surface area, and a mechanical stirrer (270 rpm). A vacuum permeate reactor connected to a vacuum pump were applied to pump out permeate by the membrane. The membrane module was cleaned for each used solution by immersion in 0.5 g/L NaOCl solution (99%, Sigma-Aldrich) for 20 minutes and 0.1M citric acid (99%, Sigma-Aldrich) solution for 15 minutes, respectively. The characteristics of leachate was analyzed using the standard procedure prescribed by the American Public Health Association [19] and presented in Table 1 . 2gL^{-1}NaCl (99%, Hebei Qige Biotechnology Co., Ltd., China) solution was used as the supporting electrolyte during electrochemical treatment.

Electrocoagulation process was conducted on a batch reactor which contained a 1L glass beaker with a graphite rod as cathode and Fe@Al electrodes as anode immersed in the aqueous solution in size of 10cm×5cm×0.1cm. The sizes of electrodes were 8cm×4cm which dipped in the electrochemical reactor to a depth of 3.0 cm. The inter-electrode distance was maintained at 2 cm. Prior the experiment, the cathode was polished with 600 grit sandpaper to eliminate adsorbed impurities and passivation layer, and then cleaned with acetone (99%, Xilong Scientific Co., Ltd., China) and ethanol (96%, Shandong Kawah Oils Co., Ltd., China), respectively to remove oil, and washed with deionized water. A peristaltic pump (504U, Watson Marlow) was connected to the electrocoagulation reactor to pump solution. 1L leachate was injected into the water cell and the solution was agitated with a magnetic stirrer by the speed of 200 rpm. Both temperature and pH of water were monitored using a pH/temperature meter (HI 98130,Hanna). The current densities of 0.2, 0.5, 1, 3, 5, 8 and 10 mA/cm^2 were applied to maintain constant the electrocoagulation time (60 minutes) corresponded to the previous studies of organic matter electrocoagulation [5, 20-23]. The electrocoagulation cell was operated under galvanostatic mode by using a DC laboratory power

supplier (Xantrex XFR40-70;0-40V, 0-70A, 2800 Watt, AcaTmetrix, Canada) to monitor and record the current intensity. The recirculation flow in the reactor was mixed with the reaction mixture during the experiment. For separation of the sludge, the treated effluent in the electrocoagulation process was filtered. The TOC analyzer (3100 TOC/TN, Analytik Jena, Germany) was used for determination of TOC removal. The COD concentration was measured using the closed refluxed, colorimetric method [19]. The removal of chromaticity in the electrocoagulation process was studied with a UV-Vis Spectrometry at 650 nm (Perkin Lambda 40, Elmer, Waltham, MA, USA).

Table 1. Landfill leachate characteristics

Property	value
TOC	102.1 mg l^{-1}
COD	387.5 mg l^{-1}
Oil and grease	21.5
pH	5.9
conductivity	3.3 mS cm^{-1}

3. RESULTS AND DISCUSSION

SEM images of electrodeposited Al NPs, Fe NPs, and Al@Fe samples presented in Figure 1. As observed from Figure1, Al and Fe samples consist of spherical nanoparticles in average size of 80 nm and 85 nm, respectively. SEM images of Al@Fe sample in Figure 1c shows nanoparticles in average size of75 nm, which are homogeneously distributed in the composite matrix. The average size of nanoparticles in nanocomposite samples is lower than Al and Fe nanoparticles samples.

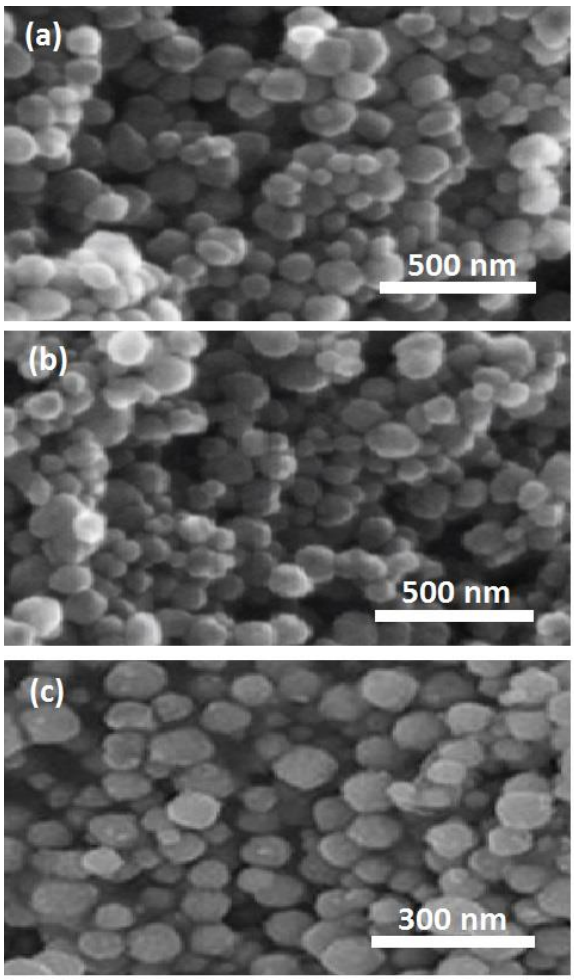

Figure 1. SEM images of the prepared powder of electrodeposited (a) Al NPs, (b) Fe NPs, (c) Al@Fesamples.

XRD powder patterns of electrodeposited Al NPs, Fe NPs, Al@Fe (4:1), Al@Fe (3:1), Al@Fe and Al@Fe (3:1) are shown in Figure 2. XRD pattern of Al NPs sample shows the diffraction peaks at 31.98° and 67.04° for (220) and (440) planes of γ-Al_2O_3, respectively with cubic structure (JPCD card No. 29-63), and the diffraction peaks at 39.01°, 44.98°, 65.52°, 78.30°and 82.35° which associated with (111), (200), (220), (311) and(222) planes of Al, respectively in fcc crystal structure (JPCD card No. 01-1180). The XRD pattern of Fe NPs sample shows the diffraction peak at 44.46° for (110) plane of polycrystalline α-iron metallic [24]. For Al@Fe (4:1), Al@Fe (3:1), Al@Fe and Al@Fe (3:1) samples, XRD patterns display the same as that of diffraction peaks of Al NPs sample with broad peak at about 44° due to present the Fe nanostructure in prepared nanocomposites.

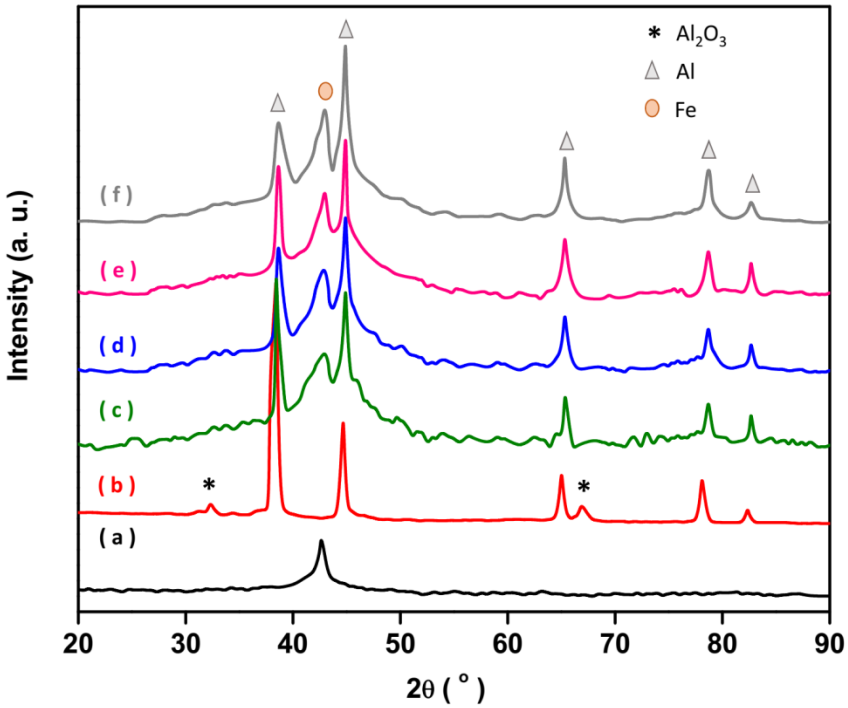

Figure 2. XRD patterns of the prepared powder of electrodeposited (a) Fe NPs, (b)Al NPs, (c) Al@Fe (4:1), (d) Al@Fe (3:1) and (e) Al@Fe and (f) Al@Fe (1:3).

The electrochemical behaviors of GCE, Al NPs/GCE, Fe NPs/GCE, Al@Fe (4:1)/GCE, Al@Fe (3:1)/GCE, Al@Fe/GCE and Al@Fe (1:3)/GCE were studied through recorded CVs in 0.1M KCl including 1mM $K_3[Fe(CN)_6]$ at 200 mV s^{-1} scan rate. Figure 3 shows the recorded CVs which indicated the redox process of $[Fe(CN)_6]^{3-/4-}$ with peak separation potential of 0.251, 0.208, 0.165, 0.179, 0.131 and 0.135 V for GCE, Al NPs/GCE, Fe NPs/GCE, Al@Fe (4:1)/GCE, Al@Fe (3:1)/GCE, Al@Fe/GCE and Al@Fe (1:3)/GCE, respectively. The lower peak separation potential and higher peak current are observed on Al@Fe/GCE which can related to its faster reversible charge transfer process than that of other electrodes due to simultaneously and equally presence of Al and Fe NPs on electrode surface and higher electrical conductivity of Fe in nanocomposite and its higher surface area [25, 26].

Figure 4 exhibits the CV curves and plot of redox peak current vs. square root of the scan rate for prepared electrode at various scan rates from 20 to 100 mV/s in 0.1M KCl including 1mM $K_3[Fe(CN)_6]$. As shown, the peak current was increased by increasing the value of scan rate. The linear relationship in plots of the peak current vs. the square root shows reaction between the electrolyte and electrode surface is quasi-reversible [27]. The efficient surface area for electrode may be calculated using the Randles–Sevcik formula [25]:

$$I_p=2.69\times10^5\, n^{3/2}AD^{1/2}C\nu^{1/2} \qquad (1)$$

Where n presents the number of electrons which transferred in redox reaction (n=1), I_p (A) shows peak current density, D (6.5×10^{-6} cm^2/s) and A (cm^2) present the diffusion-coefficient of $[Fe(CN)_6]^{3-/4-}$ and electroactive surface area, respectively. C(mol/cm^3) and ν (V/s) show electroactive

catalytic species and scan rate, respectively. Therefore, effective surface areas of Al NPs/GCE, Fe NPs/GCE, Al@Fe(4:1)/GCE, Al@Fe(3:1)/GCE, Al@Fe/GCE and Al@Fe (1:3)/GCE can be calculated 1.28×10^{-3}, 3.25×10^{-3}, 3.60×10^{-3}, 3.56×10^{-3}, 4.34×10^{-3} and 3.89×10^{-3}cm^2 respectively. Accordingly, Al@Fe/GCE sample shows the higher effective surface area. The greater the electrode surface area per reactor volume, the more efficient it is in eliminating impurities in a solution [28]. Thus, it is suggested that the Al@Fe (1:3) and Al@Fe can show a higher treatment rate than other prepared electrodes.

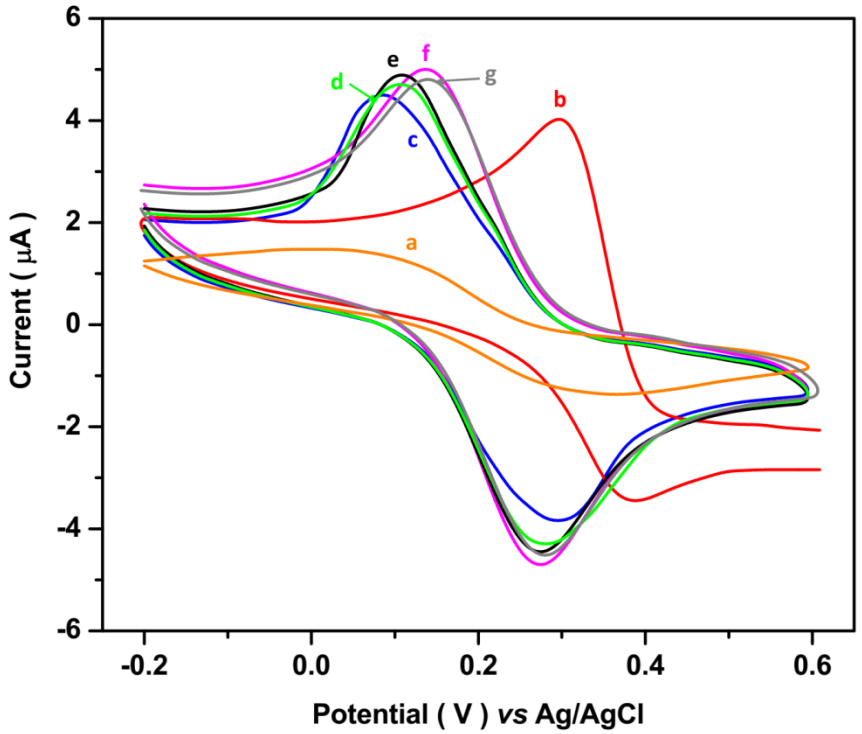

Figure 3. The CVs of (a) GCE, (b) Al NPs/GCE, (c) Fe NPs/GCE, (d) Al@Fe(4:1)/GCE, (e) Al@Fe(3:1)/GCE,(f) Al@Fe/GCE and (g) Al@Fe(1:3)/GCE in 1mM $K_3[Fe(CN)_6]$ including 0.1M KCl (pH 7) at 200 mV s^{-1} scan rate.

pH is an important parameter in the electrocoagulation cell and has effects on the solubility of metal hydroxide which is generated in the electrocoagulation step and going to act as the coagulant and remove the pollutants from the solution [29]. To study the initial pH effect on the electrocoagulation process, the pH values were adjusted ranges of 2 to 12. Figures 5a and 5b show the effect of early pH on removal of TOC and COD for Fe NPs and Al NPs electrodes, respectively. It can be seen for both electrodes, the same behaviors were presented for the treatment of TOC and COD. The maximum removal efficiency was observed at pH 6. The removal efficiencies of the COD are 87% and 91% for Fe NPs and Al NPs electrodes, respectively, and removal efficiencies of the TOC are 90% and 93%% for Fe and Al electrodes, respectively in pH 6. As seen, the better removal efficiency for both electrodes happens for acidic condition (pH < 6) due to dependence of Al^{3+}or Fe^{3+} hydrolysis on pH. At acidic condition, the freshly shaped amorphous $Fe(OH)_3$ or $Al(OH)_3$ have large surface areas that

are useful for a rapid adsorption of soluble organic pollutants and trapping of colloidal particle, and in consequence more treatment of COD and TOC [29].

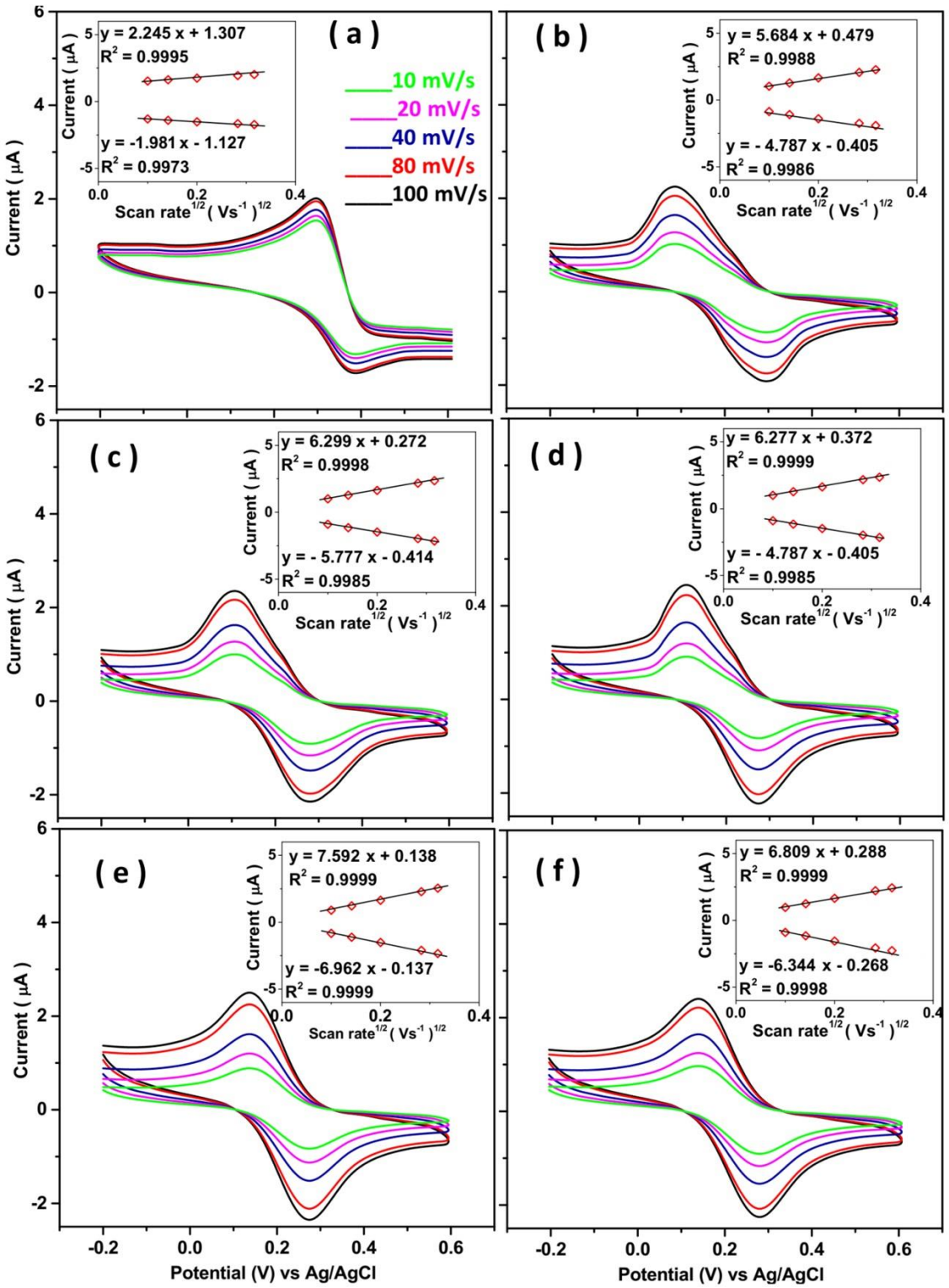

Figure 4. The CV curves and plots of redox peak current vs. square root of the scan rate for (a) Al NPs/GCE, (b) Fe NPs/GCE, (c) Al@Fe(4:1)/GCE, (d) Al@Fe(3:1)/GCE, (e) Al@Fe/GCE and (f) Al@Fe(1:3)/GCE at scan rates of 10, 20, 40, 80 and 100 mV/s in KCl (pH 7) containing 5mM $[Fe(CN)_6]^{3-/4-}$.

Studies confirmed that throughout the pH gradient (pH 4.7 and 10.5), there are polymeric aluminum hydroxides with amorphous nature and remarkable larger surface areas for pollution adsorption [30]. In alkaline condition, the dominant compounds are $Fe(OH)^{4-}$ or $Al(OH)^{4-}$ which cannot contribute to coagulate with pollutants [29]. Accordingly, following measurements were conducted on supporting electrolyte pH 6.

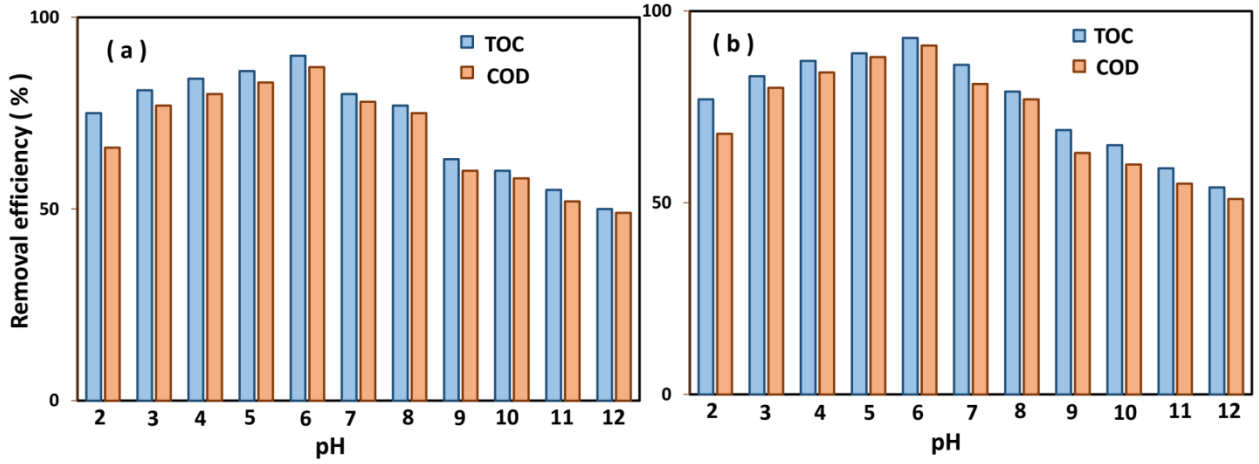

Figure 5. The initial pH effect on the COD and TOC removal efficiency through electrocoagulation process with (a) Fe NPs and (b) AlNPs electrodes in 2 gL^{-1}NaCl as supporting electrolyte, under applied current density of 1$mAcm^{-2}$ for 60 minutes at room temperature and initial concentration of COD and TOC of 387.5 mgL^{-1} and 102.1 mgL^{-1}, respectively.

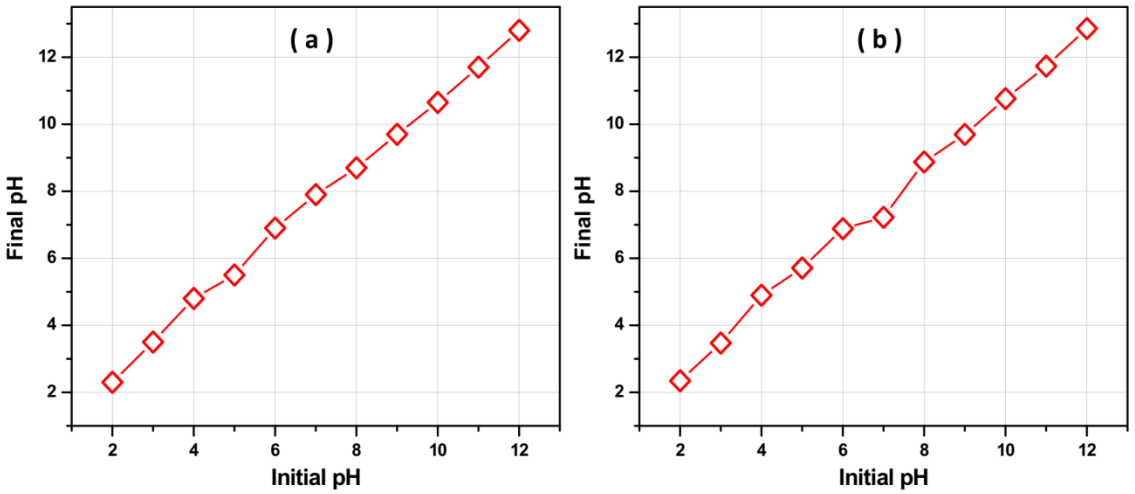

Figure 6. The pH variation *vs.* initial pH after electrocoagulation process for the TOC and COD removal with a graphite rod as cathode (a) Fe NPs and (b) Al NPs electrodes as anode in 2gL^{-1} NaCl as supporting electrolyte, under applied current density of 1 mA cm^{-2} for 60 minutes at room temperature and initial concentration of COD and TOC of 387.5 mgL^{-1} and 102.1 mgL^{-1}, respectively.

Moreover as observed from Figures 6a and 6b for both electrodes, the pH of the solution during the electrocoagulation is gradually increased. For Fe NPs electrode, the maximum flocculation values

of $Fe(H_2O)_4(OH)_2$ and $Fe_2O_3(H_2O)_6$ not only are shown at pH 6 but also maximum reduction of COD is occurred in this pH. Under the electrocoagulation process for Al NPs electrodes, different types of aluminum hydroxide species are formed depending on the pH of solution. For 5 < pH < 6, the main generated species are $Al(OH)_2^+$and $Al(OH)^{2+}$. For 5.2< pH <8.8, the predominant produced species is solid $Al(OH)_3$. For 9 < pH, $Al(OH)_4^-$ is dissolvable in water and creates the hydroxo-Al complexes [29, 31, 32].$Al(OH)_4^-$ is the only species present above pH 10 [30].

In order to determine the optimum current density on the COD and TOC removal efficiency through electrocoagulation process, the experiments were performed under applied current densities of 0.2, 0.5,1, 3, 5, 8 and10 mA cm^{-2}. Figure 7a and 7b shows the current density effect on the TOC and COD removal efficiency through electrocoagulation process with Fe NPs and Al NPs electrodes, respectively. As seen, the variation in the current density leads to change removal efficiency because of direct influence of current density on rate of bubble generation in the electrocoagulation process and hence affects the growth of created flocks which cause the treatment of pollutant in electrocoagulation process [33]. Moreover, with increasing the current density from 0.2 to 1mAcm^{-2}, the COD and TOC removal efficiencies drastically increased. Nonetheless, with raising current density from 1 to 10mA/cm^2, the removal efficiency of COD and TOC slightly increased. Therefore, the current density of 1mA/cm^2 was selected as optimum current density for following measures.

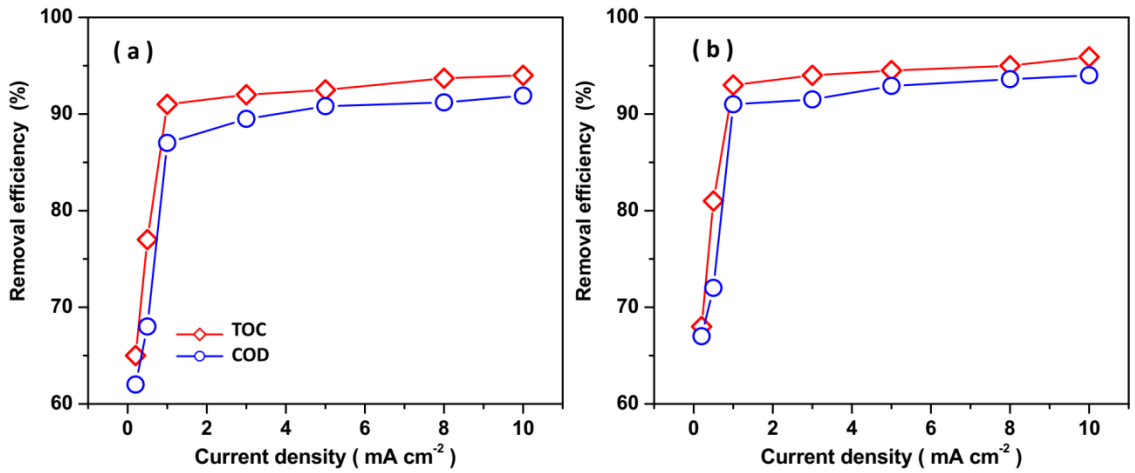

Figure 7. The current density effect on the TOC and COD removal efficiency through electrocoagulation process with a graphite rod as cathode and (a) Fe NPs and (b) Al NPs electrodeas anode in 2gL^{-1} NaCl (pH 6) as supporting electrolyte, under 60 minutes electrocoagulation at room temperature and initial concentration of COD and TOC of 387.5 mgl^{-1} and 102.1 mgL^{-1}, respectively.

Material of electrodes is another effective parameter on the efficiency of electrocoagulation [34]. Figure 8 shows the electrode material effect on electrocoagulation treatment of COD and TOC in 2gl^{-1} NaCl as supporting electrolyte, under applied current density of 1 mA cm^{-2} for 60 minutes at room temperature. As seen, Al@Fe electrode shows higher removal efficiency than other electrodes. With increasing the Fe content in nanocomposites up 50%, the removal efficiency is increased; and for

Fe content more than 50%, the removal efficiency is decreased. For Al@Fe electrodes, removal efficiency for COD and TOC are 95% and 96%, respectively. Studies showed the Fe content in electrode materials provides a higher rate of ion transfer into solution which indicates formation of higher levels of sludge [28]. This results are in agreement with the results of electrochemical studies which indicated the Al@Fe/GCE sample with the higher effective surface area can be more efficient for treatment of pollutants in a solution [28]. It is demonstrated that using Fe NPs cause to lower energy consumption whereas the electrode consumption is generally lower with aluminum. Moreover, the produced ferric ions in electrochemical oxidation of Al@Fe electrode could generate monomeric and polymeric hydroxy complexes species such as $Fe(OH)_3$, $Fe(H_2O)_6^{3+}$, $Fe(H_2O)_5(OH)_2^{+}$, $Fe(H_2O)_4(OH)_2^{+}$, $Fe_2(H_2O)_8(OH)_2^{4+}$, and $Fe_2(H_2O)_6(OH)_4^{4+}$which show the great ability to dispersed particles and counter ions to coagulation occurrence [30]. In addition, it is suggested that the smaller ionic radius of Al^{3+} (53 pm) can provide isomorphous substitution of Al^{3+} for Fe^{3+}(60 pm) in iron oxides and disrupts crystallization and forms larger surface area which would enhance adsorption [35]. Gomes et al. [30] also suggested the exchangeable Al can enhance Brønsted acidity through developing reaction of water with release H^+ ions, and adsorbed Al can behave as a Lewis acid through coordinating the moieties of some organic pollutants. It causes them to be nearer to the iron oxide surface for reductive transformations.

The electrocoagulation process fundamentally includes the metal cations dissolved from reactor anode (M: Al and Fe) under passing the current by a metal electrode and oxidizing the metals to its cation, and simultaneous reduction of water and formation of hydroxyl ion (OH^-) and H_2 at the cathode as following reactions [29, 36]:

Anode: $M \rightarrow M^+ + ne^-$ (2)

Cathode: $2H_2O\ (l) \rightarrow OH^- + H_2\ (g)$ (3)

Therefore, the dominant mechanism can vary during the dynamic process because the reaction progress, and will positively shift by changing particular pollutant types, operating parameters and treatment conditions [29, 36]. During electrocoagulation in existence of Fe and Al electrodes produces highly charged cations of Al^{3+} and Fe^{2+}or Fe^{3+}at the anode destabilizes colloidal particles through the creation of polymeric and monomeric hydroxo complex species. The metal hydroxo complexes such as iron and aluminum hydroxides remain in the aqueous-phase, and may treat the pollutant from the wastewater via electrostatic attraction or either complexation followed by coagulation thorough form strong aggregates with pollutants due to high adsorption properties [29, 36]. The amount of metal hydrolysis depends on the pH and the total metal concentrations, as well as the concentration and type of other species in the solution [37]. Accordingly, at acidic condition (pH 6), the freshly formed amorphous $Fe(OH)_3$ or $Al(OH)_3$ have large surface areas that are useful for a rapid adsorption of soluble organic pollutants and trapping of colloidal particle, and in consequence more treatment of COD and TOC.

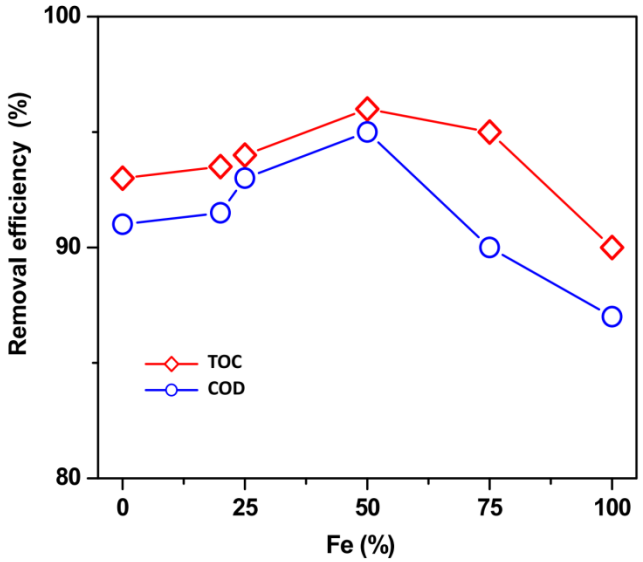

Figure 8. The electrode material effect on the TOC and COD removal efficiency through electrocoagulation process with a graphite rod as cathode and Al@Fe nanocomposite electrode with various content of Fe as anode under applied current density of 1mA/cm^2 for 60 minutes at room temperature in 2 gL^{-1}NaCl (pH 6) as supporting electrolyte, and initial concentration of COD and TOC of 387.5 mgL^{-1} and 102.1 mgL^{-1}, respectively.

4. CONCLUSION

In this study, treatment of TOC and COD from soil pollution of agricultural solid waste leachate was studied using electrocoagulation technique with Al@Fe nanocomposites electrode. Electrodeposition method in ionic liquid was employed to synthesize Al@Fe nanocomposites. Result of characterization of morphology and crystalline structure of the sample showed that surface of electrodes covered of spherical nanoparticles of Al in fcc crystal structure and Fe in polycrystalline α-iron metallic which homogeneously distributed in the composite matrix. Moreover, the effects of initial pH, current density and Fe concentration in electrode content for the electrocoagulation treatment were examined and results exhibited COD and TOC removal efficiencies were obtained 95% and 96%, respectively after 60 minutes treatment in 2gl^{-1}NaCl as supporting electrolyte under optimal condition which contained pH 6 and applied current density of 1 mA cm^{-2} at room temperature. In addition, the optimum removal efficiency was obtained using Al@Fe electrode with equal concentration of Al and Fe. Results indicated that nanostructured electrodes provided the higher effective surface for electrochemical treatment.

ACKNOWLEDGEMENT
This work was sponsored in part by the National Natural Science Foundation of China (31372245).

References

1. S. Singh, N.J. Raju, W. Gossel and P. Wycisk, *Arabian Journal of Geosciences*, 9 (2016) 131.
2. D.P. Brown, *Resources, Conservation and Recycling*, 98 (2015) 41.

3. T.J. Britz, C.A. Venter and R.P. Tracey, *Biological Wastes*, 32 (1990) 181.
4. J.B. Christensen, D.L. Jensen, C. Grøn, Z. Filip and T.H. Christensen, *Water research*, 32 (1998) 125.
5. O. Dia, P. Drogui, G. Buelna and R. Dubé, *Waste Management*, 75 (2018) 391.
6. H. Karimi-Maleh, M.L. Yola, N. Atar, Y. Orooji, F. Karimi, P.S. Kumar, J. Rouhi and M. Baghayeri, *Journal of colloid and interface science*, 592 (2021) 174.
7. H. Karimi-Maleh, S. Ranjbari, B. Tanhaei, A. Ayati, Y. Orooji, M. Alizadeh, F. Karimi, S. Salmanpour, J. Rouhi and M. Sillanpää, *Environmental Research*, 195 (2021) 110809.
8. V. Torretta, N. Ferronato, I.A. Katsoyiannis, A.K. Tolkou and M. Airoldi, *Sustainability*, 9 (2017) 9.
9. J. Rouhi, S. Kakooei, M.C. Ismail, R. Karimzadeh and M.R. Mahmood, *International Journal of Electrochemical Science*, 12 (2017) 9933.
10. R. Savari, H. Savaloni, S. Abbasi and F. Placido, *Sensors and Actuators B: Chemical*, 266 (2018) 620.
11. J. Fu, X. He, J. Zhu, W. Gu and X. Li, *International Journal of Electrochemical Science*, 13 (2018) 5872.
12. H. Karimi-Maleh, M. Alizadeh, Y. Orooji, F. Karimi, M. Baghayeri, J. Rouhi, S. Tajik, H. Beitollahi, S. Agarwal and V.K. Gupta, *Industrial & Engineering Chemistry Research*, 60 (2021) 816.
13. A. Osman, M. Elamin and M. Almalki, *Journal of Environmental & Analytical Toxicology*, 7 (2017) 2161.
14. M. Zarei, A. Niaei, D. Salari and A.R. Khataee, *Journal of electroanalytical chemistry*, 639 (2010) 167.
15. C. Weisbart, S. Raghavan, K. Muralidharan and B.G. Potter, *Carbon*, 116 (2017) 318.
16. P. Giridhar, B. Weidenfeller, S.Z. El Abedin and F. Endres, *Physical Chemistry Chemical Physics*, 16 (2014) 9317.
17. A. Ukalska-Jaruga, B. Smreczak and A. Klimkowicz-Pawlas, *Journal of Soils and Sediments*, 19 (2019) 1890.
18. E. Jamroz, J. Bekier, A. Medynska-Juraszek, A. Kaluza-Haladyn, I. Cwielag-Piasecka and M. Bednik, *Scientific Reports*, 10 (2020) 1.
19. A.P.H. Association, A.W.W. Association, W.P.C. Federation and W.E. Federation, *Standard methods for the examination of water and wastewater*. Vol. 2. 1912: American Public Health Association.
20. M. Tanyol, A. Ogedey and E. Oguz, *Water Science and Technology*, 77 (2018) 177.
21. K.D. Cruz, J.T.J. Francisco, K.J.M. Mellendrez and J.M.F. Pineda. *Electrocoagulation treatment of swine slaughterhouse wastewater: effect of electrode material*. in *E3S Web of Conferences*. 2019: EDP Sciences.
22. O. Dia, P. Drogui, G. Buelna, R. Dubé and B.S. Ihsen, *Chemosphere*, 168 (2017) 1136.
23. D.S. Ibrahim, M. Lathalakshmi, A. Muthukrishnaraj and N. Balasubramanian, *Petroleum Science*, 10 (2013) 421.
24. H.D. Omar, *Journal of Nanotechnology & Advanced Materials*, 3 (2015) 57.
25. Z. Savari, S. Soltanian, A. Noorbakhsh, A. Salimi, M. Najafi and P. Servati, *Sensors and Actuators B: Chemical*, 176 (2013) 335.
26. N. Elgrishi, K.J. Rountree, B.D. McCarthy, E.S. Rountree, T.T. Eisenhart and J.L. Dempsey, *Journal of chemical education*, 95 (2018) 197.
27. D. Thomas, Z. Rasheed, J.S. Jagan and K.G. Kumar, *Journal of food science and technology*, 52 (2015) 6719.
28. A.S. Naje, S. Chelliapan, Z. Zakaria, M.A. Ajeel and P.A. Alaba, *Reviews in Chemical Engineering*, 33 (2017) 263.

29. I. Kabdaşlı, I. Arslan-Alaton, T. Ölmez-Hancı and O. Tünay, *Environmental Technology Reviews*, 1 (2012) 2.
30. J.A. Gomes, P. Daida, M. Kesmez, M. Weir, H. Moreno, J.R. Parga, G. Irwin, H. McWhinney, T. Grady and E. Peterson, *Journal of hazardous materials*, 139 (2007) 220.
31. M. Dembowski, M.M. Snyder, C.H. Delegard, J.G. Reynolds, T.R. Graham, H.-W. Wang, I.I. Leavy, S.R. Baum, O. Qafoku and M.S. Fountain, *Physical Chemistry Chemical Physics*, 22 (2020) 4368.
32. N.P. Tanattı, İ.A. Şengil and A. Özdemir, *Applied Water Science*, 8 (2018) 58.
33. S. Adamovic, M. Prica, B. Dalmacija, S. Rapajic, D. Novakovic, Z. Pavlovic and S. Maletic, *Arabian Journal of Chemistry*, 9 (2016) 152.
34. A. Ndjomgoue-Yossa, C. Nanseu-Njiki, I. Kengne and E. Ngameni, *International Journal of Environmental Science and Technology*, 12 (2015) 2103.
35. T. Satapanajaru, S. Comfort and P. Shea, *Journal of Environmental Quality*, 32 (2003) 1726.
36. X. Chen, G. Chen and P.L. Yue, *Separation and purification technology*, 19 (2000) 65.
37. J.T.G. Overbeek, *Journal of Colloid and Interface Science*, 58 (1977) 408.